Journal of Power Sources 195 (2010) 8327–8330

Contents lists available at ScienceDirect

Journal of Power Sources

journal homepage: www.elsevier.com/locate/jpowsour

Short communication

Electrochemical characteristics of aluminum sulfide for use in lithium secondary batteries

Hiroshi Senoh[a,*], Tomonari Takeuchi[a], Hiroyuki Kageyama[a], Hikari Sakaebe[a], Masaru Yao[a], Koji Nakanishi[b], Toshiaki Ohta[b], Tetsuo Sakai[a], Kazuaki Yasuda[a]

[a] Research Institute for Ubiquitous Energy Devices (UBIQEN), National Institute of Advanced Industrial Science and Technology (AIST), 1-8-31 Midorigaoka, Ikeda, Osaka 563-8577, Japan
[b] Synchrotron Radiation Center (The SR Center), Ritsumeikan University, 1-1-1 Noji-Higashi, Kusatsu, Shiga 525-8577, Japan

ARTICLE INFO

Article history:
Received 24 May 2010
Received in revised form 22 June 2010
Accepted 23 June 2010
Available online 30 June 2010

Keywords:
Lithium secondary battery
Aluminum sulfide
Charge–discharge curve
Capacity retention
X-ray diffraction
X-ray absorption near edge structure

ABSTRACT

In our effect to develop a lithium secondary battery with high energy density, aluminum sulfide (Al_2S_3) was studied for use as an active material. The measured initial discharge capacity of Al_2S_3 was ca. 1170 mAh g^{-1} at 100 mA g^{-1}. This corresponds to 62% of the theoretical capacity for the sulfide. Al_2S_3 exhibited poor capacity retention in the potential range between 0.01 V and 2.0 V, mainly due to the structural irreversibility of the charge process or Li extraction. XRD and Al and S K-XANES analyses indicated that the surface of Al_2S_3 reacts reversibly during charge and discharge processes, while the core of Al_2S_3 showed structural irreversibility because LiAl and Li_2S were formed from Al_2S_3 at the initial discharge and remained as they were afterward.

1. Introduction

Lithium secondary batteries are widely used as electric power sources. To improve battery performance, various active materials for both anode and cathode have been investigated. Metal sulfides have been proposed as promising active materials because of their high theoretical capacities in comparison to those of currently available systems with oxide-based materials. Recently, a variety of transition metal-containing sulfides MS_2 such as M = Fe, Co, Ni and Cu have been studied as cathode materials [1–4]. Some metal sulfides can also be utilized as anode materials, which depend on the redox potentials.

With respect to *p*-block elements, some sulfides act as semiconductors. In the field of electrochemistry, lithium-containing sulfide glasses such as Li_2S–SiS_2–P_2S_5 and Li_2S–SiS_2–Al_2S_3 systems show higher ionic conductivity than the corresponding oxide glasses, which have been studied as candidates for application to solid-state electrolyte materials in lithium secondary batteries [5–9]. By taking advantage of its high ionic conductivity, GeS_2 has been considered as a new anode material for these batteries [10].

In this work, the sulfide of another element with smaller atomic number Al was studied. Although the electrochemical behaviors of Al_2S_3 in molten salts have been reported [11,12], to our knowledge, there has been no previous report on the possible application of Al_2S_3 as an active material for use in lithium secondary batteries. If we assume that Al_2S_3 is completely lithiated ($Al_2S_3 + 10.5Li^+ + 10.5e^- \rightleftarrows 0.5Li_9Al_4 + 3Li_2S$), its theoretical capacity is 1874 mAh g^{-1} or 4123 mAh cm^{-3}. In the present work, we examined the electrochemical properties of Al_2S_3, and particularly focused on the structural changes during the galvanostatic cycle.

2. Experimental

Commercially available Al_2S_3 powder (purity > 99%, Alfa) was used as-received for electrochemical studies. SEM observation indicated that the Al_2S_3 powder was a lump-like structure with a size of ca. 10 μm. A working electrode was prepared by mixing 3.5 mg Al_2S_3 powder with 1.5 mg teflonized acetylene black (TAB-2, Hohsen), and the resultant electrode was then dried in vacuo for 1 h. A charge–discharge cycle test was performed in a two-electrode system using a sealed cell (HS cell, Hohsen). The counter electrode was Li foil (Honjo). Although Al_2S_3 reacts in the potential range of anode, we evaluated it as a cathode, and the potential of the working electrode as a positive electrode is represented against (Li/Li^+). The separator and electrolyte were a

* Corresponding author. Tel.: +81 72 751 9653; fax: +81 72 751 9629.
E-mail address: h.senoh@aist.go.jp (H. Senoh).

0378-7753/$ – see front matter © 2010 Elsevier B.V. All rights reserved.
doi:10.1016/j.jpowsour.2010.06.079

porous polypropylene sheet (Asahi Kasei Chemicals) and 1 mol L^{-1} lithium hexafluorophosphate in a 1:1 mixture of ethylene carbonate and dimethyl carbonate (Kishida), respectively. The cell was constructed in an Ar-filled glove box. The cycle test was conducted at 30 °C using a charge/discharge unit (TOSCAT-3100, Toyo System). In the cycle test, the prepared cell was first discharged at a current density of 100 mA g^{-1} with a cutoff potential of 0.01 V, allowed to rest for 1 h, and then charged at the same current density with a cutoff potential of 2.0 V.

After the cycle test, the cells were disassembled inside the Ar glove box and the working electrodes were washed with dimethyl carbonate to remove the electrolyte. Ex situ X-ray diffraction (XRD) of the electrode was performed by covering it with a cellulose acetate film to avoid a reaction with moisture/air. XRD patterns were recorded with an XRD unit (X' Pert PRO MPD, PANalytical) using Cu Kα radiation. The oxidation states of the elements (Al and S) were examined by Al K-edge and S K-edge X-ray absorption near edge structure (XANES) analyses. XANES measurements were performed at BL-10 of the SR Center, Ritsumeikan University [13].

3. Results and discussion

Fig. 1 shows discharge and charge curves of Al_2S_3 electrode into which teflonized acetylene black has been incorporated. Before the initial discharge, there is no plateau region in a potential window of 2.0–4.0 V. In Fig. 1 the initial discharge curve shows a short plateau at ca. 0.6 V followed by a long plateau at ca. 0.5 V. The former shoulder is observed only at the initial discharge and is enlarged by incorporating the teflonized acetylene black. For an acetylene black, it is reported the SEI formation occurs at the initial discharge [14]. The potential decreases smoothly and the initial discharge capacity of the electrode was ca. 1390 mAh g^{-1}. In subsequent charging (second charge), the potential increases gradually. After that, two sloping plateaus are observed at ca. 0.5 V and 1.2 V during charge process and two sloping plateaus are also seen at ca. 0.1 V and 0.7 V during discharge process. With an increase in the cycle number, all plateau regions, particularly at higher plateaus during both discharge and charge processes, become narrow.

Capacity retention of Al_2S_3 after subtracting the capacity contribution from teflonized acetylene black is shown in Fig. 2. Initial discharge capacity of Al_2S_3 was ca. 1170 mAh g^{-1}. This is about 62% of the theoretical capacities for Al_2S_3. The subsequent charge capacity was ca. 650 mAh g^{-1}, which corresponds to the extraction of 3.6Li. This value is somewhat higher than the capacity of GeS_2 [10].

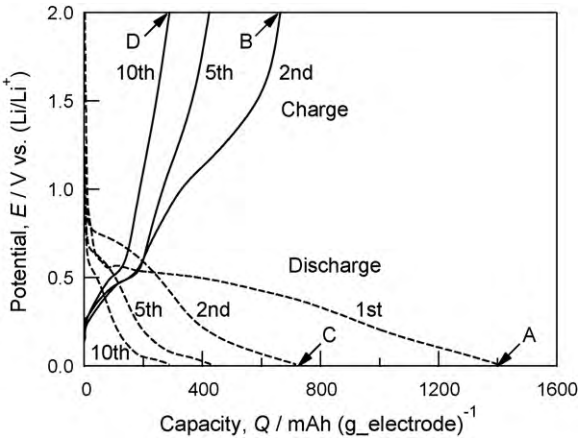

Fig. 1. Initial, second, fifth and tenth discharge–charge curves of Al_2S_3 electrode in a potential window of 0.01–2.0 V at 100 mA g^{-1}. Notations A–D correspond to those in Figs. 4–6.

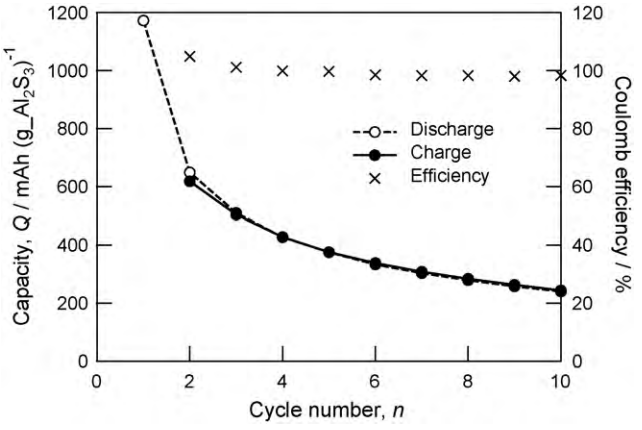

Fig. 2. Discharge and charge capacities of Al_2S_3 at 100 mA g^{-1} corrected for teflonized acetylene black and coulomb efficiency vs. cycle number.

With an increase in the cycle number, the capacities of Al_2S_3 during both discharge and charge processes degraded very rapidly to only ca. 240 mAh g^{-1} after 10 cycles. A notable point is that the discharge capacity remains comparable to the preceding charge; i.e., the coulomb efficiency of discharge against charge was almost 100%. This suggests that the drastic decrease in capacity with cycle is mainly due to the charge process or Li extraction.

Fig. 3 shows the rate capability of Al_2S_3. The initial discharge capacity at 1000 mA g^{-1} is only 33% of that at 100 mA g^{-1}. Below 500 mA g^{-1}, the initial discharge capacities show an approximately linear dependence with the current density. Discharge capacities that do not include the influence of the overpotential were estimated by extrapolation to 0 mA g^{-1}. The value obtained (1240 mAh g^{-1}) is still far from the theoretical capacity; i.e., Al_2S_3 may not react completely during the initial discharge process.

To clarify the reaction mechanism and factors that contribute to degradation of the electrode, it is important to understand the structural change of Al_2S_3 during discharge and charge processes. Fig. 4 shows ex situ XRD profiles of Al_2S_3 electrode. Before the cycle test (Before in Fig. 4), all of the diffraction peaks of Al_2S_3 are indexed according to a hexagonal structure ($P6_1$) [15]. At the end of the initial discharge (A), the diffraction peaks of Al_2S_3 decrease, while some broad peaks corresponding to Li_2S appear. In the subsequent charge (B), the relative intensities of the diffraction peaks of Al_2S_3 increase again, although those of Li_2S still remain. The diffraction peaks after the second discharge (C) are almost identical to those

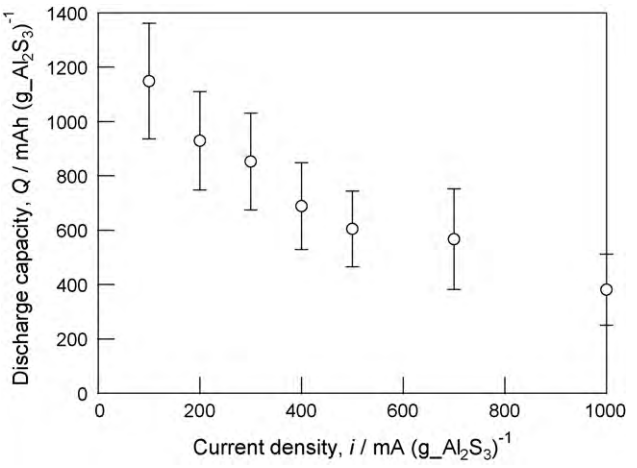

Fig. 3. Initial discharge capacity of Al_2S_3 corrected for teflonized acetylene black against current density. Error is twice of the standard deviation of the means values.

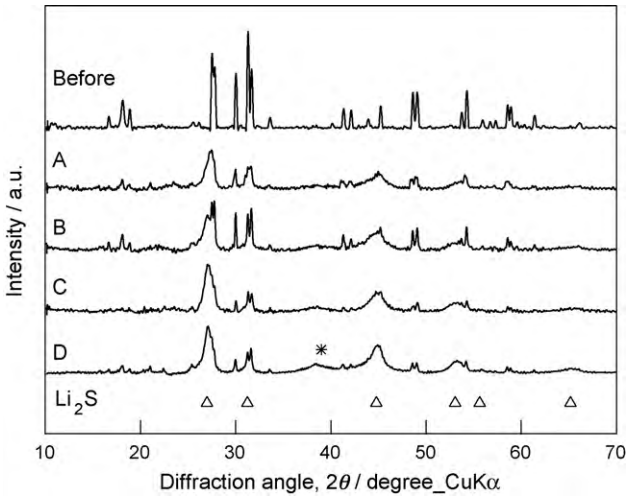

Fig. 4. Ex situ XRD profiles of Al_2S_3 electrode before cycle test and after discharge and charge. Notations A–D correspond to those in Fig. 1.

after the initial discharge (A). Li_2S as well as Al_2S_3 remain even in the charged state after 10 cycles (D). Additionally, one broad peak (* in Fig. 4 D) was observed at ca. 39°. This may be assigned to Al metal and/or Li–Al alloy because Al metal and Li–Al alloy show the strongest peaks around the broad peak (Al(1 1 1): 38.6°, LiAl(2 2 0): 40.0°, Li_9Al_4(−6 1 1): 39.1°) [16].

Structural changes were examined in greater detail by XANES analyses. Fig. 5 shows ex situ Al K-edge XANES spectra for Al_2S_3

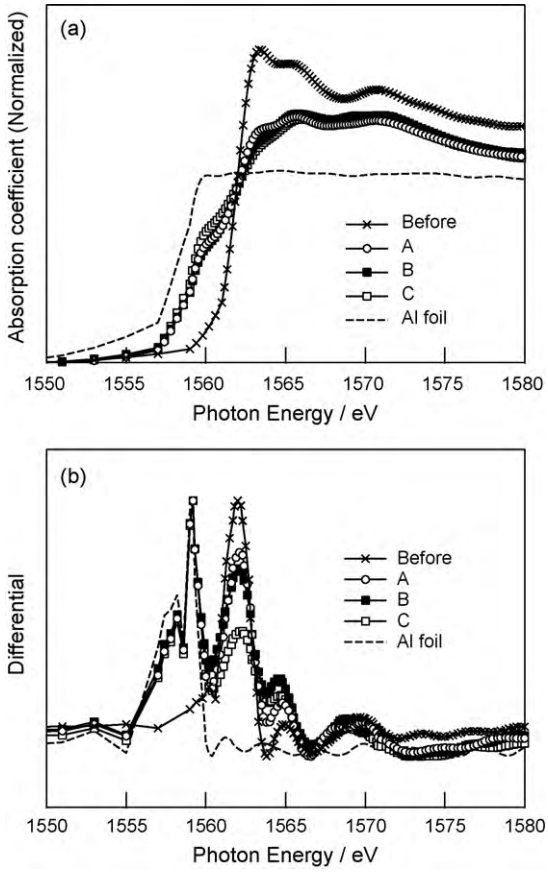

Fig. 5. Al K-edge XANES spectra for Al_2S_3 electrode in PFY mode before cycle test and after discharge and charge; normalized (a) and first differential (b). Notations A–C correspond to those in Fig. 1. Al foil was used as a reference.

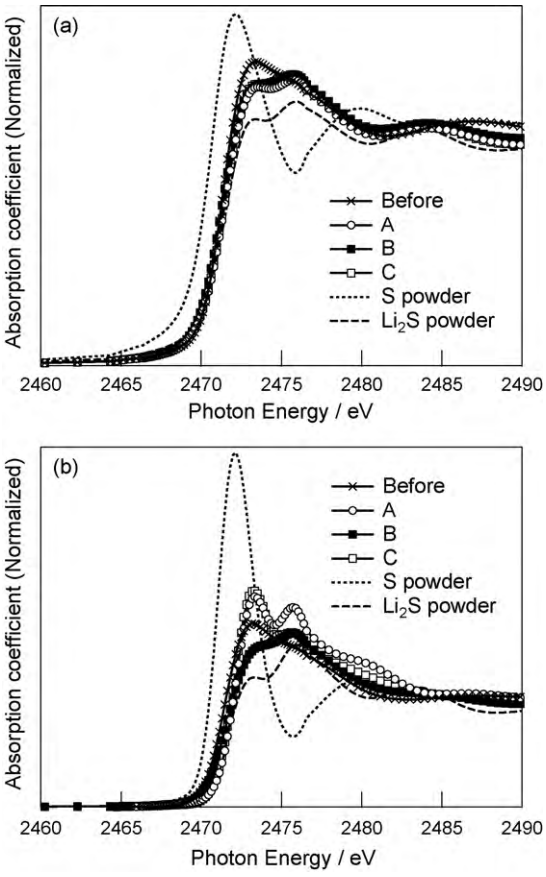

Fig. 6. S K-edge XANES spectra for Al_2S_3 electrode in PFY mode (a) and TEY mode (b) before cycle test and after discharge and charge. Notations A–C correspond to those in Fig. 1. S and Li_2S powders were used as references.

electrode obtained with the partial fluorescence yield (PFY) mode before and after the cycle test. In Fig. 5(a), the edge position of the Al K-edge XANES spectrum for Al_2S_3 electrode (Before) shifts to a lower energy after the initial discharge (A), and remains at the same energy in the subsequent charge (B). At the second discharge (C), further reduction of Al_2S_3 electrode occurs. The first differential XANES spectra (Fig. 5(b)) indicate that a peak at around 1562 eV corresponding to Al_2S_3 decreases, while peaks at around 1558 eV and 1559 eV related to Al metal appear after the cycle test. Since the PFY mode is rather bulk-sensitive, the results above suggest that, in the bulk of Al_2S_3, the average oxidation state of Al decreases with the first Li insertion, probably due to the formation of Al metal or Li–Al alloy and this remains after subsequent cycles.

Fig. 6 shows ex situ S K-edge XANES spectra for Al_2S_3 electrode before and after the cycle test. Characteristic absorption peaks at around 2473 eV originate from the S 1s → 3p electronic transition. The behaviors in the S K-edge XANES spectra measured in the PFY mode (Fig. 6(a)) are, on the whole, quite similar to those for the Al K-edge XANES spectra. The spectrum after the initial discharge (A) is similar, not to that for Al_2S_3, but rather to that for Li_2S. The lack of a significant change in the XANES spectra after the second cycle (B and C) suggests that the oxidation state of S is invariant during the cycle test. In contrast, the difference in the spectra between the discharge and charge processes is clearly observed in the total electron yield (TEY) mode (Fig. 6(b)). The peak for Al_2S_3 electrode at around 2473 eV before the cycle test shifts slightly to high energy and its intensity increases after the initial discharge (A). Note that the TEY mode is surface-sensitive, and probes surface atoms within ~10 nm. These findings suggest that, on the surface of Al_2S_3, the average oxidation state of S increases probably due

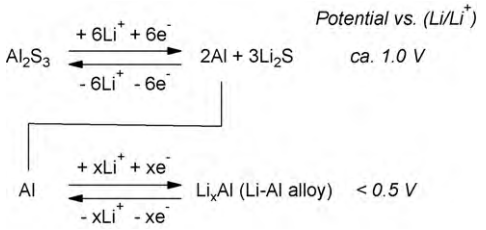

Fig. 7. Schematic representation for the proposed reaction mechanism of Al_2S_3.

to the formation of Li_2S–Al_2S_3 alloy such as $LiAl_4S_7$ and/or $LiAlS_2$ [5]. The change in the local structure during the initial discharge process may influence the S K-edge XANES spectra. The intensity of the peak at around 2476 eV related to Li_2S increases during the discharge process (A) and decreases again at recharge (B) although the spectrum of the recharged electrode does not completely overlap that of the original Al_2S_3 electrode. The peak at around 2473 eV after the second discharge (C) returns approximately to that after the initial discharge (A). This indicates a reversible reaction on the electrode surface. As shown in Fig. 6, all of the spectra have higher edge energy than that for S powder, which indicates the absence of S residue after the cycle test.

Based on the information above, it is reasonable to speculate that the reaction mechanism for Al_2S_3 mainly consists of two steps (Fig. 7). At the initial discharge, Al_2S_3 is converted into Li_2S and Li_xAl (Li–Al alloy). For a Li–Al system, Jow and Liang [17] reported the effect of the composition on the electrode potential of Li–Al alloys. In the present study, the discharge–charge curves with a pair of plateaus below 0.5 V in Fig. 1 approximately agree with the electrode potential in their report, and an equilibrium potential after the initial discharge (ca. 0.15 V) corresponds to the stability region of the LiAl phase in the Li–Al system. This indicates that the composition of the Li–Al alloy is probably not Li_9Al_4 ($x = 2.25$) but rather LiAl ($x = 1$) and the reaction $Al + Li^+ + e^- \rightleftarrows LiAl$ occurs at the lower potential during charge and discharge processes. For the higher plateaus during charge and discharge processes, the midpoint between the potentials (0.7 V and 1.2 V) shown in Fig. 1 agrees fairly well with the equilibrium potential of the reaction $Al_2S_3 + 6Li^+ + 6e^- \rightleftarrows 2Al + 3Li_2S$ (1.01 V at 25 °C), calculated from thermodynamic data [18,19]. In addition, the equilibrium potential of Li_2S/S is 2.25 V [20], which is greater than the potential window in the present study. These findings suggest that the reaction $Al_2S_3 + 6Li^+ + 6e^- \rightleftarrows 2Al + 3Li_2S$ occurs at higher potential during charge and discharge processes.

As mentioned above, the drastic decrease in capacity during the cycle test is mainly due to Li extraction. The results of XRD and XANES analyses suggest that the surface of Al_2S_3 reacts reversibly during charge and discharge processes, while the core of Al_2S_3 shows structural irreversibility because LiAl and Li_2S are formed from Al_2S_3 at the initial discharge and remain as they are afterward. The diffusion of Li in LiAl alloy is quite slow [17], which leads to the poor reactivity of Li. Moreover, Li_2S shows no significant capacity (electrochemically inactive) due to poor electronic conductivity [21]. The partial solubility of Li_2S into the electrolyte may be another factor in the fading of capacity retention [20]. As shown in Fig. 1, the higher plateaus become particularly narrow during both the discharge and charge processes, which is attributed to the irreversible reaction of Li_2S. These observations would be responsible for the degradation of the cycle capability in the present Li/Al_2S_3 cells. Therefore, finer Al_2S_3 particles would be anticipated to suppress the formation of LiAl and/or Li_2S and improve the cycle capability. Studies on the preparation of finer Al_2S_3 particles are currently underway.

4. Summary

The electrochemical characteristics of Al_2S_3 for use in lithium secondary batteries were investigated using galvanostatic cycle. The prepared electrode showed a high initial capacity although the capacity retention was insufficient. It is reasonable to speculate that the reaction mechanism for Al_2S_3 mainly consists of two steps; $Al_2S_3 + 6Li^+ + 6e^- \rightleftarrows 2Al + 3Li_2S$ and $Al + Li^+ + e^- \rightleftarrows LiAl$. The lithiated reaction of Al_2S_3 occurs at low potential, which is a good reason for selecting the sulfide as an anode material.

Acknowledgements

The authors are grateful to their colleagues at the Research Institute for Ubiquitous Energy Devices for their helpful suggestions and stimulating discussions, especially Dr. N. Fujiwara, Dr. T. Ioroi, Dr. Z. Siroma, Dr. S. Yamazaki and Dr. N. Takeichi. We also wish to thank Ms. J. Hirai and Mr. S. Ohta for their helpful assistance. Part of this work was financially supported by the R&D project for Li batteries by NEDO.

References

[1] R. Fong, J.R. Dahn, C.H.W. Jones, J. Electrochem. Soc. 136 (1989) 3206–3210.
[2] A. Débart, L. Dupont, R. Patrice, J.M. Tarascon, Solid State Sci. 8 (2006) 640–651.
[3] J.M. Yan, H.Z. Huang, J. Zhang, Z.J. Liu, Y. Yang, J. Power Sources 146 (2005) 264–269.
[4] T. Takeuchi, H. Sakaebe, H. Kageyama, T. Sakai, K. Tatsumi, J. Electrochem. Soc. 155 (2008) A679–A684.
[5] E.E. Hellstrom, R.A. Huggins, Mater. Res. Bull. 14 (1979) 881–889.
[6] K. Takada, N. Aotani, S. Kondo, J. Power Sources 43–44 (1993) 135–141.
[7] S.M. Martin, J.A. Sills, J. Non-Cryst. Solids 135 (1991) 171–181.
[8] M. Maruyama, R. Kanno, M. Irie, S. Ito, T. Hata, N. Sonoyama, Y. Kawamoto, Solid State Ionics 168 (2002) 140–148.
[9] A. Hayashi, T. Fukuda, H. Morimoto, T. Minami, M. Tatsumisago, J. Mater. Sci. 39 (2004) 5125–5127.
[10] Y. Kim, H. Hwang, K. Lawler, S.W. Martin, J. Cho, Electrochim. Acta 53 (2008) 5058–5064.
[11] N.Q. Minh, R.O. Loutfy, N.P. Yao, J. Electroanal. Chem. 131 (1982) 229–242.
[12] V.A. Dusheiko, J. Power Sources 97–98 (2001) 555–556.
[13] K. Nakanishi, T. Ohta, J. Phys.: Condens. Matter 21 (2009) 104214.
[14] M.V.V.M. Satya Kishore, U.V. Varadaraju, J. Power Sources 156 (2006) 594–597.
[15] B. Krebs, A. Schiemann, M. Laege, Z. Anorg. Allg. Chem. 619 (1993) 983–988.
[16] A.V. Trifonova, A.A. Momchilov, B.L. Puresheva, I. Abrahams, Solid State Ionics 143 (2001) 319–328.
[17] T.R. Jow, C.C. Liang, J. Electrochem. Soc. 129 (1982) 1429–1434.
[18] J.G. Speight (Ed.), Lange's Handbook of Chemistry, 16th ed., McGraw-Hill, New York, 2005.
[19] Kagaku-Binran, The Electrochemical Society of Japan Ed., 5th ed., Maruzen, Tokyo, 2000.
[20] T. Takeuchi, H. Sakaebe, H. Kageyama, H. Senoh, T. Sakai, K. Tatsumi, J. Power Sources 195 (2010) 2928–2934.
[21] M.N. Obrovac, J.R. Dahn, Electrochem. Solid State Lett. 5 (2002) A70–A73.